BIOINSPIRED LIQUID METAL BASED SENSING SYSTEM FOR COMPLIANCE DETECTION

Haotian Chen[1], Ivan Furfaro[1], and Stéphanie P. Lacour[1]
[1]Laboratory for Soft Biolectronic Interfaces, Center for Neuroprosthetics,
EPFL, Geneva, Switzerland

ABSTRACT

In this paper, we report a fully stretchable liquid metal based sensor system for compliance detection. The system is composed of a strain sensor layer, a gap layer with a hole in the center and a pressure sensor layer from top to bottom. Inspired from the human tactile system, the pressure sensor and strain sensor work collaboratively to detect the force and deformation simultaneously, from which the compliance of the contact material can be derived.

KEYWORDS

Liquid metal, stretchable sensor system, thin film; multi-modal sensing

INTRODUCTION

Electronic skins are artificial sensory systems that aim at mimicking the mechanical properties of human skin and its multisensory modalities [1], [2]. The ability of humans to discriminate softness or compliance of an object relies on tactile inputs of the skin mechanoreceptors and manipulation (squeeze or stroke) of the object. Such perception allows us to judge whether a fruit is ripe or the tire of a bicycle is flat. Although a rather subjective sensation, which varies across humans, softness perception finds important implementation in haptics and robotics.

From the mechanical engineering point of view, human skin can be regarded as a 2 dimensional (2D) surface. So generally, the interaction between the human skin and an object is a 2D-2D interaction, where the stimuli can be divided into two types, vertical stimuli and tangential stimuli. By analyzing these two basic stimuli, compliance detection is available.

In the past decades, researchers have developed a plethora of stretchable mechanical sensors with high performance and employing various materials [3], [4]. Among them, liquid metals, especially gallium-based liquid metal, have emerged as an ideal electrical skin-like material combining high stretchability and high electrical conductivity [5]. Gallium based liquid metals and associated alloys exhibit low vapor pressure and good stability. Once embedded into a silicone carrier, liquid metals follow pre-arranged patterns and form highly deformable interconnects, antenna and sensors.

In this paper, we propose a soft, skin-like, sensor system composed a strain sensor layer, a gap layer with a hole in the center and a pressure sensor layer. All of sensors are resistive and made from liquid metal encapsulated by polydimethylsiloxane (PDMS). The liquid metal is deposited by thermal evaporation thereby forming thin conductive film e.g. 1.5 µm. The total thickness of the sensor system, consisting of the 3 functional layers, is only 0.5 mm, which is compatible with an easy integration at the surface of various objects, which in turn acquire smart sensing ability. By coupling pressure and strain sensors, this skin-like system captures simultaneously force and deformation, thus obtaining inform on the compliance of the touched material. This first prototype is macroscopic with a 6.25 cm^2 surface area (Fig. 1a).

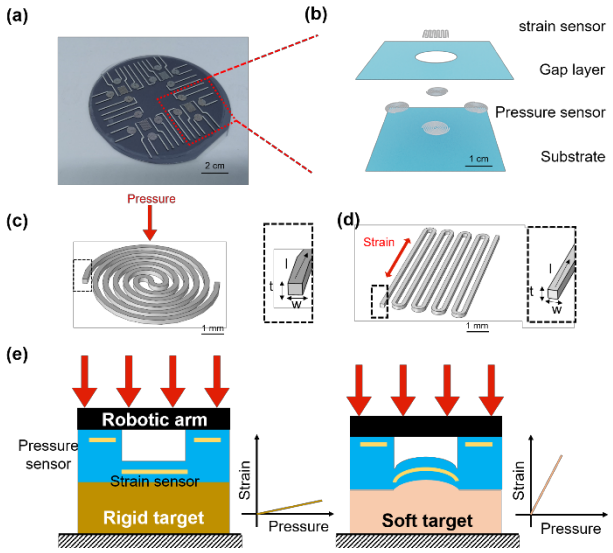

Figure 1: Working mechanism and design of the compliance sensor. (a) Photography of the sensor system on 4 inch silicon wafer; (b) The schematic diagram of the sensor system configuration containing laminated layers; The schematic diagram of pressure sensor (c) and (d); (e) Working mechanism of the sensor system composed of strain sensor and pressure sensor.

SENSOR SYSTEM DESIGN

Compliance

Stiffness is the extent to which an object resists deformation in response to an applied force. Conversely, compliance c is the inverse of stiffness k defined as

$$\boldsymbol{k = F/x} \qquad (1)$$

Where, F is the force on the body and x is the displacement produced by the force along the same direction.

The compliance of the object is function of the elastic property of the material (Young's modulus, E) and its geometry [6]. To sense the compliance of the object, we then need to measure both the applied force and resulting deformation. To do so, we introduce a sensor system that includes a normal force sensor and a strain sensor.

Sensor structure

Figure 1(a) displays a photography of four sensor systems fabricated on 4 inch silicon wafer. Each sensor system contains four pressure sensors in a cross arrangement and one freestanding strain sensor at the center (Figure 1(b)). The pressure sensor is a spiral shape

with an outer radius of 2.5 mm and the strain sensor is in meander pattern and rectangle shape (5.5 mm × 7.5 mm). The width of all liquid metal traces is 200 µm. The diameter of the hole below the strain sensor is 4 mm.

The working mechanism of the sensors is simple. As the device is pressed or stretched, the liquid metal embedded in the PDMS deforms and the resistance changes due to the reduced cross-sectional area and increased length, assuming incompressibility of the liquid metal. Here, we assume the resistivity of liquid metal is affected with the applied mechanical loading. Then, the resistance change (ΔR) before and after pressing or stretching can be found as follows:

$$\Delta \mathbf{R} = \frac{\boldsymbol{\rho l}}{\boldsymbol{tw}}\left(\frac{\boldsymbol{\Delta l}}{\boldsymbol{l}} - \frac{\boldsymbol{\Delta t}}{\boldsymbol{t}} - \frac{\boldsymbol{\Delta w}}{\boldsymbol{w}}\right) \quad (2)$$

Where ρ is electrical resistivity of Gallium, l is the length of liquid metal trace, t and w are thickness and width of liquid metal, respectively.

Specifically, for the spiral sensor shown Figure 1(c), the normal pressure mainly induces a compression along t and expansion in l and w. Introducing the Poisson coefficient of PDMS in equation (2), the resistance change of pressure sensor (ΔR_p) can be written as:

$$\Delta \boldsymbol{R_p} = \frac{\boldsymbol{\rho l}}{\boldsymbol{tw}}\left(-\boldsymbol{\nu}\frac{\boldsymbol{\Delta t}}{\boldsymbol{t}} - \frac{\boldsymbol{\Delta t}}{\boldsymbol{t}} + \boldsymbol{\nu}\frac{\boldsymbol{\Delta t}}{\boldsymbol{t}}\right) = \frac{\boldsymbol{\rho l}}{\boldsymbol{tw}}\frac{\boldsymbol{\sigma}}{\boldsymbol{E}} \quad (3)$$

Similarly, for the strain sensor shown Figure 1(d), applied strain along the length of the sensor increases l but decreases w and t. Therefore, the resistance change of strain sensor (ΔR_s) can be described as:

$$\Delta \boldsymbol{R_s} = \frac{\boldsymbol{\rho l}}{\boldsymbol{tw}}(\mathbf{1} + \mathbf{2}\boldsymbol{\nu})\frac{\boldsymbol{\Delta l}}{\boldsymbol{l}} \quad (4)$$

According to (5) and (6), the highest resistance change with applied mechanical load is obtained for long, thin and narrow metallic tracks.

Working mechanism

The compliance sensing operation is described Figure 1(e). The sensor system is targeted to be mounted on a rigid structure such as a robotic arm and the objects to be detected are assumed to have a flat and smooth surface. As the sensing unit touches the target object, each pressure sensor detects the applied load in vertical direction while the central strain sensor in senses the beam flexure in extension mode in the tangential direction. The combined outputs of the 5 sensors are able to inform on the touched object compliance. In the case of a rigid object, the deformation in strain sensor is almost zero as there is almost no deformation from the object because of its high stiffness as shown in Figure 1(e) (left). In this case, the output of the strain sensor is very low compared to the one from the pressure sensor. While as the robotic hand moves to a soft object, there will be a larger deformation in the surface because of lower stiffness, which will make the strain sensor bend (Figure 1(e), right). In this case, the ratio between the strain sensor output and pressure sensor output will be relatively larger. By comparing the ratio of the strain sensor and pressure sensor, which represent deformation and force, respectively, the compliance of the target object can be inferred.

FINITE-ELEMENT MODELING

To better understand the working mechanism and identify important geometrical and material features of the sensors and predict the sensors' output as a function of the stiffness of the object, we adopted a finite-element model based on COMSOL Multiphysics software. In order to mimic the real application, the model contains three parts, a robotic arm, the sensor system and the target object from top to bottom as shown Figure 2(a) (top). In the sensor system, the pressure sensor and strain sensor are located at different regions (SS' for strain sensor and PP' for pressure sensor). 1 kPa pressure is applied on top of robotic arm and bottom of target object is fixed. Figure 2(a) (bottom) shows the simulation of the sensor system and soft target object (E=10^4 Pa) deforming under pressure; this corresponds to the schematic diagram in Figure 1(e) (right).

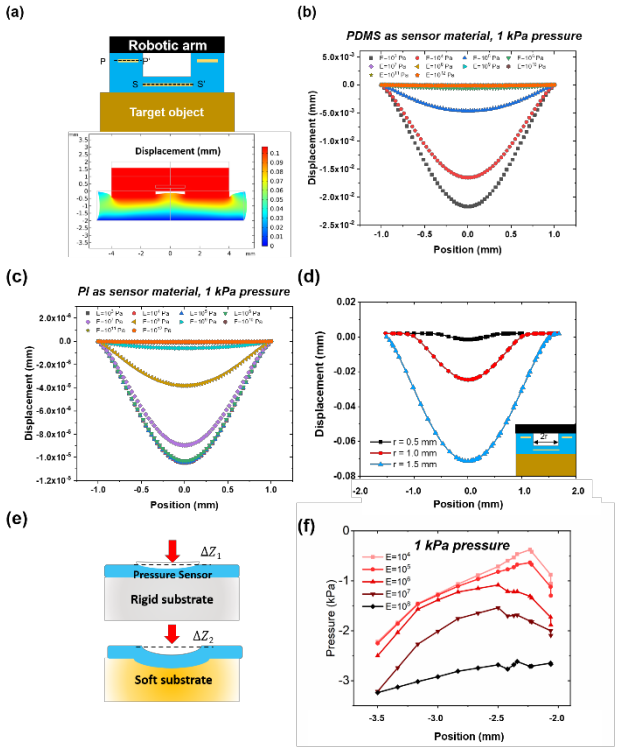

Figure 2: Finite element simulation of the sensor system. (a) Schematic diagram of the simulation model (top) and simulation result of when softer material is touched by the sensor (bottom); Displacement of the strain sensor in PDMS (b) or PI (c) pressed on objects with different Young's modulus under 1 kPa pressure; (d) Simulation results of how radius of the circular opening influence the deformation of strains sensor; (e) Schematic diagram of how the compliance of substrate may influence the pressure sensor; (f) Simulation results demonstrating how objects with different Young's modulus influence the pressure in pressure sensor region.

Based on the boundary conditions mentioned above, we first investigate how the strain sensor deforms when pressured by objects with different Young's modulus (from 10^3 Pa to 10^{12} Pa) (Figure 2(b)). We observe 2 regimes: when the target object is softer than the PDMS that forms the structural material of the sensor system, large deflections are observed; When the target object is stiffer than PDMS (E > 10^6 Pa), only small deformation occurs.

This was expected and similar to human tactile function. For instance, it is easier for people to feel that jelly ($E \sim 10^4$ Pa) is softer than rubber ($E \sim 10^6$ Pa) than distinguish glass ($E \sim 70$ GPa) from iron ($E \sim 200$ GPa). Of note, the effective Young's modulus of human skin is around 10^6 Pa. To further verify this idea, we simulate the sensor system based on polyimide (PI, $E = 2.5$ GPa) instead of PDMS. Results are displayed in Figure 2(d). The absolute deformation of the sensor embedded in PI is much lower than that of the sensor in PDMS. Soft sutrctural material enables higher sentivity. Moreover, PI only has higher resolution of differentiating materials with Young's modulus from 10^6 Pa to 10^9 Pa, which verifies the idea that the sensor's identify range is related to the material of the sensor itself.

Then we study the how the strain sensor's deformation is influenced by the size of the hole (r) in the gap layer. This is particularly important when the object is softer than the sensor. The simulation results is shown in Figure 2(d). When the radius increases from 0.5mm to 1.5mm, the deflection of the strain sensor increases by >10 times when it is pressed on a target material with a Young's modulus of 10^4 Pa: this result suggests that the increase of the hole size is able to improve the sensitivity dramatically when detecting compliance material.

For the pressure sensor in the system, the compliance of the target object also influences its output. As shown in Figure 2(e), when the pressure sensor is on a rigid object, the deformation is almost inside the sensor itself. However, then the pressure sensor is on a soft substrate, both the sensor and the substrate deform under pressure. As the pressure sensor is based on the geometry change, the difference of deformation will influence the output of the sensor. The simulation results of pressure distribution in the pressure sensor region shown in Figure 2(f) confirm this conclusion when the sensor is placed onto materials with Young's modulus ranging from 10^4 Pa to 10^8 Pa under 1 kPa pressure. According to the simulation, if the target material is stiffer than PDMS, the pressure tends to accumulate inside the sensor, which causes the pressure larger than the given load. Oppositely, when the target material is softer than PDMS, the target object is easier to deform than the sensor, thus the pressure at the sensor region is smaller. This phenomena suggests that the pressure sensor cannot precisely detect a given load if the target material compliance varies. In order to solve this problem, calibration is necessary, which will be discussed in the following section.

FABRICATION

As shown with eq. (3 & 4), patterning thin gallium films with high-resolution is beneficial for sensors performance. But it is always a challenge to pattern gallium because of its high surface tension and poor adhesion to elastomer. In the previous works [7], an effective method was proposed by engineering the PDMS surface with microscopic pillars to improve the adhesion and enable a wafer-scale manufacture as shown Figure 3(a). The thin and uniform liquid metal film is coated by thermal evaporation [8]. Figure 3(b) demonstrates that gallium forms uniform and smooth film on textured PDMS.

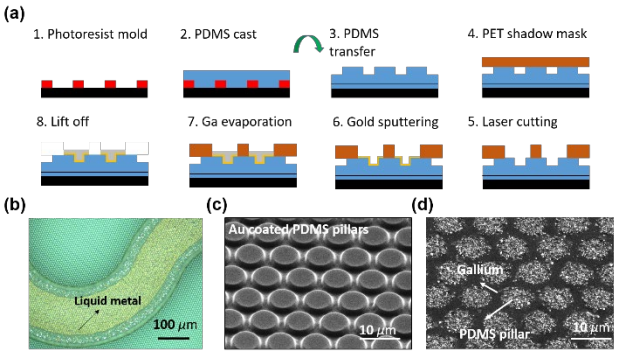

Figure 3: Fabrication of the thin film liquid metal based sensors. (a) Thin film liquid metal manufacturing process; (b) Liquid metal deposited on flat PDMS surface and textured PDMS surface; (c) SEM image of the textured PDMS; (d) SEM image of liquid metal deposited onto textured PDMS forming a thin and uniform surface.

In details, the silicon wafer carrier was treated with an adhesion promoter and then spin-coated with a 1.5 μm-thick layer of photoresist. After exposure, development and post bake, the photoresist will work as the mold for the following steps. To form the textured silicone substrate, PDMS was spin-coated as an 80 μm-thick film on photoresist and cured at 80 °C for 2 hours. Then the PDMS was transferred to another wafer with PDMS, which enables the textured PDMS is flat enough on the new carrier. 23 μm-thick polyethylene terephthalate (PET) shadow mask was patterned by laser-cutting and laminated on the textured PDMS. Followed by 40 nm gold sputtered (Figure 3(c)) on the PDMS surface acting as an adhesive layer, 2 g of gallium was evaporated to fill the textured PDMS, which may form a uniform and smooth surface (Figure 3(d)). In the end, the PET shadow mask was removed and 80 μm-thick PDMS was spin-coated as the encapsulation layer. The thickness of liquid metal can be precisely controlled by the thickness of the PDMS pillars. The PDMS gap layer (100 μm) is created by laser cutting. After fabricating each layer, they are stacked to each other by plasma bonding with alignment.

RESULTS AND ANALYSIS

Four kinds of commonly used materials (commercial rubber, PDMS, Ecoflex and hydrogel) with different Young's modulus, are utilized for the test. Following the setup shown in simulation, the sensor system is equipped onto a precisely controllable robotic arm, which was utilized to apply given loads through materials of different modulus. Figure 4(a) shows the deformation-force curves of the four materials, in which the slopes represent the compliance of each material. The responses of the strain sensor when it touches the four flat materials are shown in Figure 4(b). The curve is compatible with the deformation-force curves from the materials, which verifies that this sensor system is able to distinguish the compliance in a high resolution. When it comes to the pressure sensor, the slope of its response curve varies when the target material changes (Figure 4(c)) as discussed in the simulation. In this case, the pressure sensor itself is unable to detect the accurate load.

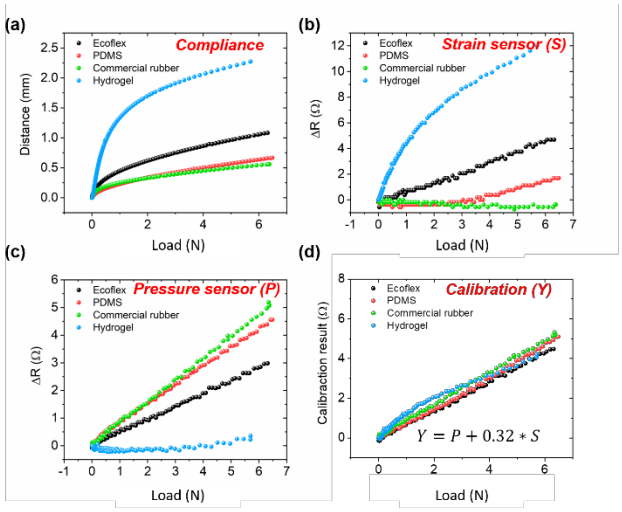

Figure 4: Characterization of the sensor system. (a) Stress-strain curves of Ecoflex, PDMS, commercial rubber and hydrogel; (b) Responses of strain sensor to materials of different modulus; (c) Responses of pressure sensor to materials of different modulus; (d) Normalized results based on both strain sensor and pressure sensor.

Inspired from human tactile system, in which the different mechanoreceptors work together to provide plenty and accurate information, a coupling calibration algorithm based on the two types of sensors is developed. When the sensor system is touching a soft material, the output of pressure sensor is smaller while the one of strain sensor is larger. However, as the sensor system is contacted with a stiff material, the output of pressure sensor is larger while strain sensor's output is smaller. Intuitively, the response from strain sensor is able to provide a feedback for pressure sensor to calibrate it to real load. After large amount times of real test, a formula based on the readout from pressure sensor (P), strain sensor (S) and the real load is established. the calibration results (Y) are shown in Figure 4(d).

$$\boldsymbol{Y = P + 0.32S} \qquad (3)$$

In this way, by coupling the results from the two sensors, no matter what kind of material is touched by the robotic arm, the real load can be calculated. Once the real load is known, the compliance can be obtain by comparing the ratio of deformation and load, which correspond to S and Y, respectively.

CONCLUSION

Normally, the pressure sensor and the strain sensor have been developed independently to display the normal pressure and the deformation, respectively. However, by correlating each value in the bi-layered pressure and strain sensor, the external load can be calibrated and further the Young's modulus of the target object can be obtained.

This paper presents the fully stretchable sensor system, which consists of the pressure sensor layer, the strain sensor layer, and the gap layer in between, to detect the compliance of the target object. Both sensors are fabricated by the liquid metal and the elastomer as resistive sensors and a carrier substrate/encapsulation, respectively. We investigated soft resistive sensors for pressure and strain detection and confirmed the working principle of their combination to quantify compliance. Equipped onto a robotic arm, materials of varying compliance were tested by coupling the responses from strain sensor and pressure sensor, which demonstrates its potential applications in robotics or prosthetics.

ACKNOWLEDGEMENTS

The authors acknowledge the financial support from the Bertarelli Foundation and SNSF NCCR Robotics.

REFERENCES

[1] B. T. Nghiem *et al.*, 'Providing a sense of touch to prosthetic hands', *Plast. Reconstr. Surg.*, vol. 135, no. 6, pp. 1652–1663, Jun. 2015.

[2] R. S. Dahiya, G. Metta, M. Valle, and G. Sandini, 'Tactile Sensing—From Humans to Humanoids', *IEEE Transactions on Robotics*, vol. 26, no. 1, pp. 1–20, Feb. 2010.

[3] H.-R. Lim, H. S. Kim, R. Qazi, Y.-T. Kwon, J.-W. Jeong, and W.-H. Yeo, 'Advanced Soft Materials, Sensor Integrations, and Applications of Wearable Flexible Hybrid Electronics in Healthcare, Energy, and Environment', *Advanced Materials*, vol. 32, no. 15, p. 1901924, 2020.

[4] M. L. Hammock, A. Chortos, B. C.-K. Tee, J. B.-H. Tok, and Z. Bao, '25th Anniversary Article: The Evolution of Electronic Skin (E-Skin): A Brief History, Design Considerations, and Recent Progress', *Advanced Materials*, vol. 25, no. 42, pp. 5997–6038, 2013.

[5] M. D. Dickey, 'Stretchable and Soft Electronics using Liquid Metals', *Advanced Materials*, vol. 29, no. 27, p. 1606425, 2017.

[6] L. Beker *et al.*, 'A bioinspired stretchable membrane-based compliance sensor', *PNAS*, May 2020.

[7] L. Dejace, N. Laubeuf, I. Furfaro, and S. P. Lacour, 'Gallium-Based Thin Films for Wearable Human Motion Sensors', *Advanced Intelligent Systems*, vol. 1, no. 5, p. 1900079, 2019.

[8] A. Hirsch, H. O. Michaud, A. P. Gerratt, S. de Mulatier, and S. P. Lacour, 'Intrinsically Stretchable Biphasic (Solid–Liquid) Thin Metal Films', *Advanced Materials*, vol. 28, no. 22, pp. 4507–4512, 2016.

CONTACT

*Stéphanie P. Lacour, stephanie.lacour@epfl.ch